Evidence of Partial Seniority Conservation in the $\pi g_{9/2}$ Shell for the $N = 50$ Isotones

R. M. Pérez-Vidal,[1,2,*] A. Gadea,[1] C. Domingo-Pardo,[1] A. Gargano,[3] J. J. Valiente-Dobón,[2] E. Clément,[4] A. Lemasson,[4] L. Coraggio,[3,5] M. Siciliano,[6] S. Szilner,[7] M. Bast,[8] T. Braunroth,[8] J. Collado,[9] A. Corina,[10] A. Dewald,[8] M. Doncel,[11] J. Dudouet,[12] G. de France,[4] C. Fransen,[8] V. González,[9] T. Hüyük,[1,13] B. Jacquot,[4] P. R. John,[14] A. Jungclaus,[13] Y. H. Kim,[4,15] A. Korichi,[16] M. Labiche,[17] S. Lenzi,[18,19] H. Li,[4] J. Ljungvall,[16] A. López-Martens,[16] D. Mengoni,[18,19] C. Michelagnoli,[4,15] C. Müller-Gatermann,[6,8] D. R. Napoli,[2] A. Navin,[4] B. Quintana,[20] D. Ramos,[4] M. Rejmund,[4] E. Sanchis,[9] J. Simpson,[17] O. Stezowski,[12] D. Wilmsen,[4] M. Zielińska,[21] A. J. Boston,[22] D. Barrientos,[23] P. Bednarczyk,[24] G. Benzoni,[25] B. Birkenbach,[8] H. C. Boston,[22] A. Bracco,[25,26] B. Cederwall,[27] D. M. Cullen,[28] F. Didierjean,[29] J. Eberth,[8] A. Gottardo,[2] J. Goupil,[4] L. J. Harkness-Brennan,[22] H. Hess,[8] D. S. Judson,[22] A. Kaşkaş,[30] W. Korten,[21] S. Leoni,[25,26] R. Menegazzo,[19] B. Million,[25] J. Nyberg,[31] Zs. Podolyak,[32] A. Pullia,[26,25] D. Ralet,[4] F. Recchia,[18,19] P. Reiter,[8] K. Rezynkina,[29,19] M. D. Salsac,[21] M. Şenyiğit,[30] D. Sohler,[33] Ch. Theisen,[21] and D. Verney[16]

[1]*Instituto de Física Corpuscular, CSIC-Universidad de Valencia, Valencia E-46980, Spain*
[2]*INFN Laboratori Nazionali di Legnaro, I-35020 Legnaro, Italy*
[3]*INFN Complesso Universitario di Monte S. Angelo, Via Cintia, I-80126 Napoli, Italy*
[4]*Grand Accélérateur National d'Ions Lourds, CEA/DRF-CNRS/IN2P3, F-14076 Caen cedex 5, France*
[5]*Dipartimento di Matematica e Fisica, Università degli Studi della Campania "Luigi Vanvitelli", viale Abramo Lincoln 5, I-81100 Caserta, Italy*
[6]*Physics Division, Argonne National Laboratory, Lemont, 60439 Illinois, USA*
[7]*Ruder Bošković Institute, 10000 Zagreb, Croatia*
[8]*Institut für Kernphysik, Universität zu Köln, D-50937 Köln, Germany*
[9]*Departamento de Ingeniería Electrónica, Universitat de Valencia, Burjassot, E-46100 Valencia, Spain*
[10]*Department of Chemistry, Simon Fraser University, Burnaby, British Columbia BC V5A 1S6, Canada*
[11]*Department of Physics, Stockholm University, SE-106 91 Stockholm, Sweden*
[12]*Université Lyon, Université Claude Bernard Lyon 1, CNRS/IN2P3, IP2I Lyon, F-69622 Villeurbanne, France*
[13]*Instituto de Estructura de la Materia, CSIC, Madrid, E-28006 Madrid, Spain*
[14]*Institut für Kernphysik, Technische Universität Darmstadt, 64289 Darmstadt, Germany*
[15]*Institut Laue-Langevin, 71 Avenue des Martyrs, 38042 Grenoble, France*
[16]*IJCLab Orsay, IN2P3-CNRS, Université Paris-Saclay and Université Paris-Sud, 91405 Orsay, France*
[17]*STFC Daresbury Laboratory, Daresbury, Warrington WA4 4AD, United Kingdom*
[18]*Dipartimento di Fisica e Astronomia dell'Università di Padova, I-35131 Padova, Italy*
[19]*INFN Sezione di Padova, I-35131 Padova, Italy*
[20]*Laboratorio de Radiaciones Ionizantes, Universidad de Salamanca, E-37008 Salamanca, Spain*
[21]*Irfu, CEA, Université Paris-Saclay, F-91191 Gif-sur-Yvette, France*
[22]*Oliver Lodge Laboratory, The University of Liverpool, Liverpool L69 7ZE, United Kingdom*
[23]*CERN, CH-1211 Geneva 23, Switzerland*
[24]*The Henryk Niewodniczański Institute of Nuclear Physics, Polish Academy of Sciences, ul. Radzikowskiego 152, 31-342 Kraków, Poland*
[25]*INFN Sezione di Milano, I-20133 Milano, Italy*
[26]*Dipartimento di Fisica, Università di Milano, I-20133 Milano, Italy*
[27]*Department of Physics, KTH Royal Institute of Technology, SE-10691 Stockholm, Sweden*
[28]*Nuclear Physics Group, Schuster Laboratory, University of Manchester, Manchester M13 9PL, United Kingdom*
[29]*Université de Strasbourg, CNRS, IPHC UMR 7178, F-67000 Strasbourg, France*
[30]*Department of Physics, Ankara University, 06100 Besevler—Ankara, Turkey*
[31]*Department of Physics and Astronomy, Uppsala University, SE-75120 Uppsala, Sweden*
[32]*Department of Physics, University of Surrey, Guildford GU2 7XH, United Kingdom*
[33]*Institute for Nuclear Research, Atomki, 4001 Debrecen, P.O. Box 51, Hungary*

(Received 31 July 2021; revised 8 February 2022; accepted 29 July 2022; published 7 September 2022)

The reduced transition probabilities for the $4_1^+ \to 2_1^+$ and $2_1^+ \to 0_1^+$ transitions in ^{92}Mo and ^{94}Ru and for the $4_1^+ \to 2_1^+$ and $6_1^+ \to 4_1^+$ transitions in ^{90}Zr have been determined in this experiment making use of a multinucleon transfer reaction. These results have been interpreted on the basis of realistic shell-model calculations in the $f_{5/2}$, $p_{3/2}$, $p_{1/2}$, and $g_{9/2}$ proton valence space. Only the combination of extensive lifetime information and large scale shell-model calculations allowed the extent of the seniority conservation in the $N = 50$ $g_{9/2}$ orbital to be understood. The conclusion is that seniority is largely conserved in the first $\pi g_{9/2}$ orbital.

DOI: 10.1103/PhysRevLett.129.112501

Seniority was introduced by G. Racah, in the context of the pairing interaction to classify states of n electrons in the atom [1]. It was shown later that seniority symmetry is applicable to any two-body interaction between identical fermions [2,3]. This concept was extended within the generalized seniority scheme for both degenerate and nondegenerate configurations of several orbitals [4,5]. The eigenstates of the pairing interaction are characterized by the seniority quantum number υ, i.e., the number of alike nucleons in every single j orbital that are not in $J = 0$ pairs [6]. Seniority is conserved if the angular momentum j of the fermions satisfies $j \leqslant 7/2$. It has been suggested that the seniority conservation is a consequence of a geometric phase (the Berry phase) associated with the particle-hole conjugation [7]. For orbitals with larger angular momenta, $j \geqslant 9/2$, seniority breaking effects may be observed being the eigenstates' admixtures of states with different seniorities [6]. The first nuclear orbital where this may occur is $g_{9/2}$ [8]. Nevertheless, in this orbital, seniority could still be conserved for a subset of solvable eigenstates. This property can be viewed as a partial dynamic symmetry [9]. The first $g_{9/2}$ orbital is found at the Fermi level in the $N = 50$ isotones toward ^{100}Sn for protons and in the $Z = 28$ neutron-rich isotopes toward ^{78}Ni for neutrons [10–12]. Nuclei in both chains have valence nucleons, protons or neutrons, respectively, occupying the same orbitals and are expected to present similarities in their structure. This situation is known as valence-mirror symmetry [13]. Seniority conservation is a result of the underlying residual interaction, which also plays a fundamental role in determining configuration mixing [6,9,13,14]. Therefore, the study of the seniority conservation in $N = 50$ isotones with valence protons filling the $g_{9/2}$ orbital may supply a testing ground for the residual interaction in the valence-mirror symmetry partners ($Z = 28$, $N \sim 50$) that, being largely neutron-rich nuclei, are expected to display sizeable differences in the residual interaction with respect to the neutron-deficient partners ($Z \sim 50$, $N = 50$). The main reason for these differences is that the $Z = 28$ proton shell gap is relatively weak as compared with the $N = 50$ neutron shell gap, which leads to distinct core-polarization effects [13].

In the $(g_{9/2})^4$ or $(g_{9/2})^{-4}$ configurations (with either neutrons or protons), two special states with good seniority $\upsilon = 4$ and total spins $J = 4$ and 6 exist for any interaction (as shown from a purely algebraic analysis [6,15]). These two $\upsilon = 4$ special states are expected to lie just above the yrast seniority $\upsilon = 2$ $J = 4$ and 8 states, respectively [9]. In addition, even for an interaction that does not preserve seniority, $\Delta\upsilon = 2$ mixing with the yrast $J = 4$, 6 states is strongly inhibited due to the large energy gap. This leads to a structure that exhibits both $\upsilon = 2$ and $\upsilon = 4$ levels and shows the same spectra and electric quadrupole ($E2$) transition properties that are obtained with a seniority-conserving interaction.

Within a pure $(g_{9/2})^4$ or $(g_{9/2})^{-4}$ configuration, the sequence of $B(E2)$ values [relative to the $B(E2; 2_1^+ \to 0_1^+)$ of the two-particle system], shown in Refs. [9,16], follows a pattern with hindered $E2$ transition probabilities between $\upsilon = 2$ states, while the $E2$ transition probabilities between the $J = 4$ and 6 states with $\upsilon = 4$ are sizable. The $E2$ transition probabilities with $\Delta\upsilon = 2$ are also expected to be large. It is important to remark that the seniority of the underlying states influences the $E2$ transition probabilities, as illustrated in Ref. [16]. Therefore, the seniority conservation hypothesis [6] should be experimentally tested via the measurement of all the $E2$ reduced transition probabilities along the yrast cascade to the maximum spin alignment. Presently, the missing experimental information on the $E2$ transition properties of the $J^\pi = 2^+$, 4^+ yrast states, along the $N = 50$ isotones, prevents one from reaching a conclusion on the partial seniority conservation in the $g_{9/2}$ shell. Lifetime measurements for the yrast 4^+ states exists only for ^{96}Pd [17] and ^{94}Ru [18], while for the yrast 2^+ states there is limited information, being available only for ^{92}Mo and ^{90}Zr [19]. Moreover, several works suggesting seniority conservation and nonseniority conservation in this region have been published over the years [13,16,17,20,21].

In order to study the seniority conservation in the proton $g_{9/2}$ orbital for the semimagic $N = 50$ isotones, lifetimes of several states in ^{90}Zr, ^{92}Mo, and ^{94}Ru have been measured for the first time at the Grand Accélérateur d'Ions Lourds (GANIL) laboratory, in Caen (France). The nuclei of interest belong to the neutron-deficient region of the nuclide chart, which is typically populated via fusion-evaporation reactions. However, with such a mechanism, medium- to high-spin states are usually reached, which

increases the difficulty of the direct lifetime measurement of the yrast states, especially in the presence of isomers. On the other hand, multinucleon transfer (MNT) reactions, broadly used to produce moderately neutron-rich nuclei, are known to populate lower angular momentum, with sizeable direct feeding [22,23]. In our Letter MNT reactions were used to populate the states of interest [24,25]. A ^{92}Mo beam with an energy of 717 MeV, accelerated by the GANIL cyclotron complex, impinged on an enriched ^{92}Mo target of thickness 0.775 mg/cm^2. The target was mounted on the IKP Cologne plunger [26], while a 1.9 mg/cm^2 thick ^{24}Mg foil was used to degrade the energy of the reaction products to measure the lifetime with the Recoil Distance Doppler Shift (RDDS) technique [26].

In this experiment, the Advanced GAmma Tracking Array (AGATA) [27,28] was coupled to the VAriable MOde Spectrometer (VAMOS++) [29,30] permitting a precise selection of the reaction products of interest and the clean observation of the γ rays emitted in coincidence. The AGATA subarray was composed of 23 HPGe crystals electrically 36-fold segmented, located 22.8 cm distance from the target and positioned at backward angles with respect to the beam direction. The digitally recorded signals from the AGATA detectors were treated with pulse shape analysis techniques [31] to extract the position of the γ-ray interaction points in the detector. This information was used to reconstruct the γ-ray path inside AGATA via tracking algorithms [32]. The AGATA position sensitivity is important in these experiments, in which the requirements of VAMOS++ for the reaction product identification limits the difference between the velocity before and after the degrader. The AGATA data sorting was performed using the GRID computing resources as detailed in Ref. [33].

The VAMOS++ spectrometer was positioned at 23° with respect to the beam axis, i.e., the grazing angle where the production cross section for the quasielastic channels is largest. The detector system of VAMOS++ provides the necessary information (energy, velocity, position, and scattering angle) for the complete ion identification in terms of the mass A, element Z, and charge state q, which is performed via an event-by-event reconstruction of the trajectory through the spectrometer [30,34,35]. Using the velocity vector of the ions in combination with the information provided by the γ-ray tracking of AGATA, the γ rays in coincidence were Doppler corrected event by event. In addition, the use of VAMOS++ allows one to limit or reduce the contribution of the indirect feeding to the state of interest by means of a condition in the detected ion, total kinetic energy loss (TKEL) [22,36,37].

The plunger device was placed in the geometrical center of the reaction chamber and perpendicular to the optical axis of the spectrometer. Seven target-to-degrader distances [19.3(9), 25.2(15), 105.2(14), 505.1(22), 1000(10), 2000(20), and 4000(40) μm] were used in order to cover the full lifetime range expected for the states in the isotones of interest (from 1 ps up to hundreds of ps). The RDDS technique is a well-established method for the determination of lifetimes in the range of picoseconds to hundreds of picoseconds [26]. The degrader slowed down the reaction products yielding two components in the γ-ray spectrum due to the different velocities (before and after the degrader) of the emitted nuclei. The distributions of velocities before and after the degrader were centered at $\beta_{\mathrm{bef}} \sim 12\%$ and $\beta_{\mathrm{aft}} \sim 11\%$, respectively. The lifetimes of the excited states were determined by two different analysis methods using the Bateman equations: fitting the decay curve (DCM) and applying the Differential Decay Curve Method (DDCM) in singles [26]. In both methods the ratio ($R_u = I_u/I_s + I_u$) of the intensities of the shifted I_s (before the degrader) and unshifted I_u (after the degrader) components as a function of the distance was evaluated. The validity of our techniques was tested with the lifetime measurement, via the two different methods (DCM and DDCM), of the $25/2^-$ excited state in ^{93}Tc [$\tau_{\mathrm{DCM}} = 79(5)$ ps and $\tau_{\mathrm{DDCM}} = 78.4(23)$ ps], 12^+ in ^{94}Ru [$\tau_{\mathrm{DCM}} = 37(8)$ ps and $\tau_{\mathrm{DDCM}} = 36(4)$ ps] and the first 4^+ state in ^{94}Mo [$\tau_{\mathrm{DCM}} = 7.1(17)$ ps and $\tau_{\mathrm{DDCM}} = 7.1(10)$ ps] using a condition in the TKEL. The results are in agreement with previously reported values [19]. Concerning the population of long-lived states in ^{92}Mo [6^+, $E_{6^+} = 2612$ keV, $\tau_{6^+} = 1.53(4)$ ns, and 5^-, $E_{5^-} = 2526$ keV, $\tau_{5^-} = 1.55(4)$ ns] and ^{94}Ru [5^-, $E_{5^-} = 2624$ keV, $\tau_{5^-} = 0.51(5)$ ns] [19], they contributed to bias the feeding of both the shifted and unshifted components due to the geometrical contribution to the line shape [38]. When necessary a subtraction of the contribution of long-lived feeding to the intensities was performed. The two procedures have been tested with the lifetime of the 4_1^+ state in ^{92}Mo (see Table I). Examples of the spectra as a function of the distance, for various distances, and the corresponding fit to the data for the de-excitation of the 4_1^+ state in ^{92}Mo (with a TKEL condition) and ^{94}Ru (with a subtraction of the feeding contribution) are shown in the left panels of Figs. 1 and 2, respectively. The experimental curves for the DCM and DDCM methods are represented together with their corresponding fits in the right panel of Figs. 1 and 2.

The lifetimes determined in this Letter and the adopted values are summarized in Table I. The corresponding reduced transition probabilities $B(E2)_{\mathrm{exp}}$ and previously measured values $B(E2)_{\mathrm{prev}}$ are also reported. Most of the $B(E2)$ strengths are in good agreement with the values and limits available from previous experiments. For the 4_1^+ state in ^{94}Ru, the present lifetime measurement does not agree with the previous limit [17] and the recent value [18] measured with the ultrafast-timing technique. After the publication of Ref. [18], stringent tests on the TKEL condition and feeder subtraction correction have been performed with the present data. These tests led to limits

TABLE I. Measured mean lifetimes τ of the exited state J^π and reduced transition probabilities $B(E2; J^\pi \to J^\pi - 2)$.

Nucleus	J^π	τ_{DCM} (ps)	τ_{DDCM} (ps)	τ_{adopted} (ps)	$B(E2)_{\mathrm{exp}}$ (e^2 fm^4)	$B(E2)_{\mathrm{prev}}$ (e^2 fm^4)
^{90}Zr	$4_1^{+\,a}$	4.3(7)	4.2(4)	4.2(4)	304(29)	…
	$6_1^{+\,a,c}$	18^{+6}_{-8}	18^{+5}_{-8}	18^{+5}_{-8}	122^{+34}_{-54}	…
	$2_1^{+\,a,c}$	0.59(15)	…	0.59(15)	196(56)	206(12)[19]
^{92}Mo	$4_1^{+\,a}$	35.5(24)	34.6(14)	35.5(6)	84.3(14)	< 304 [19]
	$4_1^{+\,b}$	36.6(13)	35.7(7)			
^{94}Ru	$2_1^{+\,b,c}$	0.8(4)	…	0.8(4)	165(80)	≥ 10 [18]
	$4_1^{+\,b}$	89(16)	87(8)	87(8)	38(3)	103(24) [18]

[a]Lifetime determined using a TKEL condition.
[b]Lifetime determined using subtraction (see text for details).
[c]Systematic errors have been taken into account when having contaminated transitions and for the short lifetimes.

between 72 ps and 95 ps for the lifetime of the 4_1^+ state in ^{94}Ru, proving the robustness of the present result.

On the other hand, the large uncertainties in $B(E2; 2_1^+ \to 0_1^+)$ of ^{92}Mo and ^{94}Ru arises from the limitation of the RDDS technique for the short lifetimes. In Fig. 3, the experimental excitation energies of the yrast states [19] (circles in top panels) and the experimental $B(E2)$ strengths of the yrast transitions from the present Letter and previous experiments [17,19,39] (circles in bottom panels) are reported for nuclei with $N = 50$ and $Z \geq 40$. In order to understand the extent of the seniority conservation in the $N = 50$ $g_{9/2}$ orbital, the combination of extensive lifetime information and shell-model calculations using a realistic interaction in a large model space is crucial.

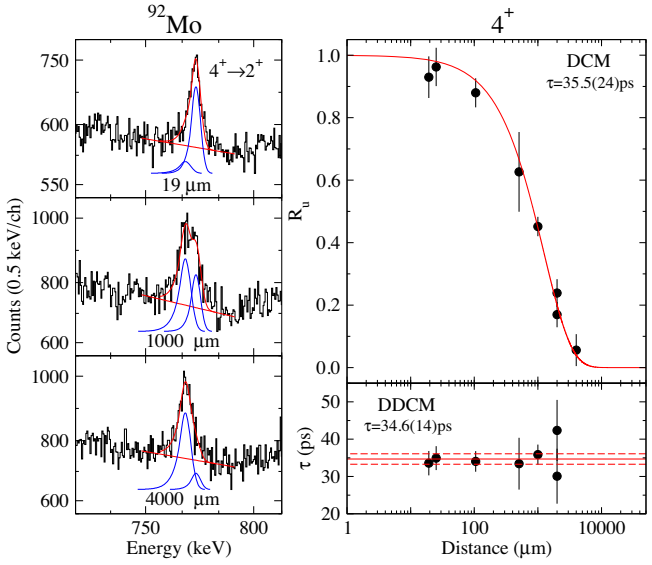

FIG. 1. Left: experimental Doppler corrected γ-ray spectra for ^{92}Mo for three target-to-degrader distances. The solid lines indicate the fit of the two components before and after the degrader. Right: lifetime determination of the 4_1^+ state in ^{92}Mo. See text for more details.

Shell-model calculations based on realistic effective interactions, that go beyond the description in the single $g_{9/2}$ shell [9], have been performed for the $N = 50$ isotones within the $f_{5/2}$, $p_{3/2}$, $p_{1/2}$, and $g_{9/2}$ model space above the ^{56}Ni core. The code ANTOINE has been used [42]. The single proton and neutron energies are taken from the experimental spectrum of ^{57}Cu and ^{57}Ni, respectively, except for the $g_{9/2}$ proton orbital that is not yet observed, and an estimated effective single particle energy of 3.2 MeV is used. It is worth noting that the presence of neutrons, which completely fill the 28–50 shell, simply affects the proton effective single particle energies. The residual two-body interaction is obtained within the many-body perturbation starting from the CD-Bonn NN potential as described in Ref. [43]. The $E2$ transition probabilities are calculated by using both empirical and microscopic effective charges. The first one uses a standard empirical effective charge of $e_\pi = 1.5e$. The microscopic effective

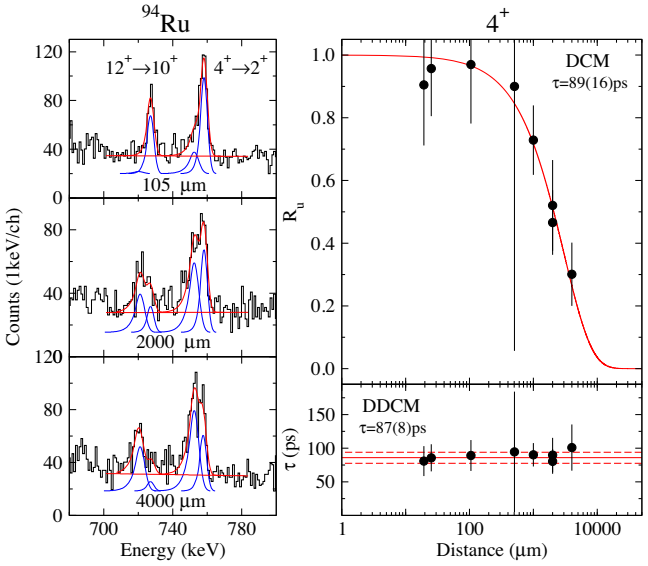

FIG. 2. Same as Fig. 1, but for the 4_1^+ state in ^{94}Ru.

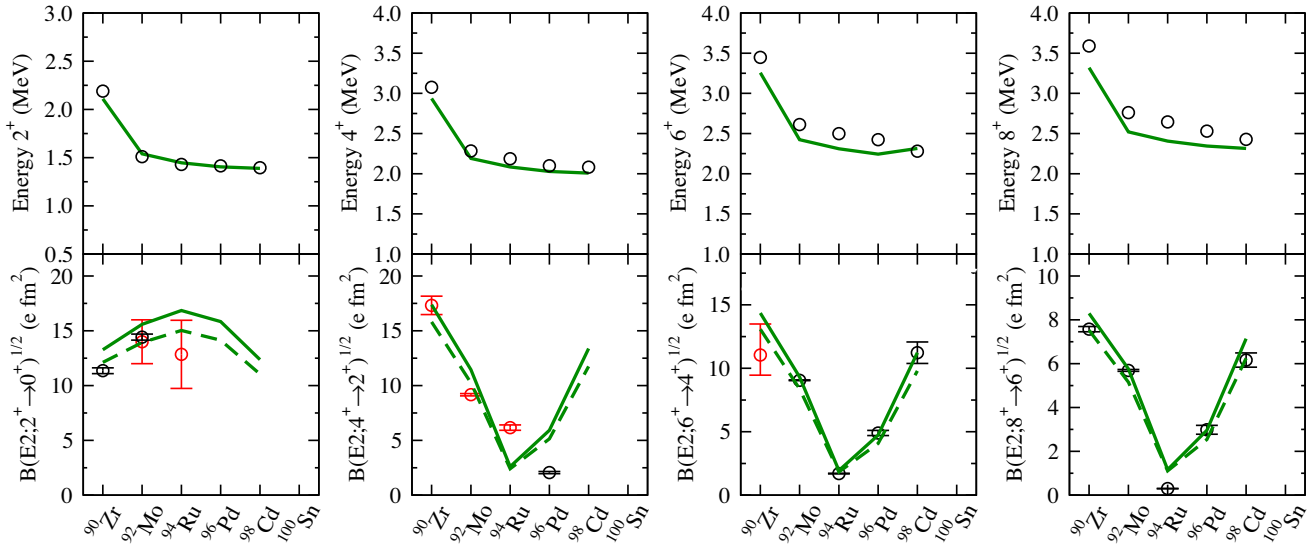

FIG. 3. Top: experimental and theoretical excitation energies of the 2^+, 4^+, 6^+, and 8^+ yrast states for $N = 50$ isotones with $A \geq 90$. The black circles are the experimental energy values [19]. The green solid lines are the shell-model predictions made for this Letter. Bottom: experimental and theoretical $B(E2; 2_1^+ \to 0_1^+)$, $B(E2; 4_1^+ \to 2_1^+)$, $B(E2; 6_1^+ \to 4_1^+)$, and $B(E2; 8_1^+ \to 6_1^+)$ values for $N = 50$ isotones with $A \geq 90$. The red circles are the experimental results of this Letter. The black circles are the experimental values from previous experiments, $B(E2; 2_1^+ \to 0_1^+)$ [19], $B(E2; 4_1^+ \to 2_1^+)$ [17], $B(E2; 6_1^+ \to 4_1^+)$ [17,19,40], and $B(E2; 8_1^+ \to 6_1^+)$ [19,41]. The green dashed (solid) lines show the shell-model calculations performed using empirical effective charges (microscopic effective charges). See text for details.

proton charges are calculated consistently with the shell-model Hamiltonian by following the Suzuki-Okamoto formalism [44,45], and their values are state dependent ranging from 1.8 to 1.3e. Both theoretical results of our shell-model calculations are depicted in green in Fig. 3.

The theoretical results account very well for all the excitation energies of the yrast states and for most of the $E2$ reduced transition probabilities in the $N = 50$ isotonic chain. The theoretical $B(E2; 2_1^+ \to 0_1^+)$ and $B(E2; 4_1^+ \to 2_1^+)$ probabilities, as confirmed by the experimental values obtained for the first time in this Letter, exhibit, respectively, a maximum and a minimum located around the half filled proton $g_{9/2}$ orbital. The former is the typical behavior for transitions with $\Delta v = 2$ in single-j systems while the latter accounts for transitions that conserve seniority ($\Delta v = 0$). The same latter pattern is observed in the systematics for the $6_1^+ \to 4_1^+$ and $8_1^+ \to 6_1^+$ transitions. Indeed, for the $N = 50$ isotones above ^{90}Zr, where the proton $g_{9/2}$ orbital is being filled, calculations predict that the 2_1^+, 4_1^+, 6_1^+, and 8_1^+ states essentially conserve seniority. The percentage of the $v = 0$ component in the ground states is larger than 98%, while the percentage of the $v = 2$ component in excited states is between 88% and 90% in ^{92}Mo and beyond 96% in ^{94}Ru, ^{96}Pd, and ^{98}Cd. The deviations between theory and experiment observed for the $4_1^+ \to 2_1^+$ transition in ^{94}Ru and ^{96}Pd may indicate that a seniority mixing larger than that resulting from our calculations is required to explain the nature of the 4_1^+ state in these nuclei. As discussed in Ref. [16], slight variations of the cross orbital nondiagonal interaction matrix elements may induce quite relevant changes in the wave function structure. On the other hand, some deficiencies in our calculations might originate from the limitations of the adopted model space. However, the solution adopted in Ref. [17], reducing the model space below $N = 50$ to the $g_{9/2}$ orbital and adding $N = Z = 50$ cross shell excitations disagrees not only with our $B(E2; 2_1^+ \to 0_1^+)$ and $B(E2; 4_1^+ \to 2_1^+)$ measurements in ^{94}Ru but also with the $B(E2; 6_1^+ \to 4_1^+)$ measurement reported for this nucleus [19]. Nevertheless, the overall picture that emerges from the present Letter is that the yrast states in ^{92}Mo, ^{94}Ru, ^{96}Pd, and ^{98}Cd may be considered within a good approximation as $v = 2$ states. In particular, the dominant $v = 2$ nature of the 4_1^+ and 6_1^+ states in ^{94}Ru and ^{96}Pd may be a direct consequence of the partial seniority conservation in orbitals with $j > 7/2$, such as the $g_{9/2}$ orbital, which prevents the mixing with the $v = 4$ even if they predicted to be just 400 keV apart. This situation is quite different in the valence-mirror symmetry partners (neutron-rich Ni isotopes), which are less known. Although theoretical calculations in this region predicted that there was an inversion of the seniority [6,13,14,46], recent measurements [11] suggest that the normal seniority ordering is recovered for ^{74}Ni up to spin $J = 4$.

In summary, the experimental $B(E2)$ values along the yrast cascade to the maximum alignment follow the expected pattern for $\Delta v = 0$ transitions. The involved wave functions are almost pure $\nu = 2$ states, and they do not mix

with nearby states with $\nu = 4$, as expected even in a simple single-shell $g_{9/2}$ model. Therefore, it can be concluded that the seniority is a good quantum number, i.e., is largely conserved, along the $(\pi g_{9/2})^n$ yrast states at $N = 50$. The experimental evidence of the seniority conservation is direct evidence of the validity of the short-range pairing interaction, with far-reaching implications for nuclear structure in the validity of BCS theory and therefore of the quasiparticle representation of the atomic nucleus [47]. Moreover, our realistic shell-model study within the proton $f_{5/2}$, p, $g_{9/2}$ model space may give grounds to compare the seniority properties of the valence-mirror symmetry partners ^{78}Ni – ^{100}Sn $N = 50$ isotones and $^{56-78}$Ni $Z = 28$ isotopes. Indeed, shell-model predictions for the Ni isotopic chain indicate that seniority might not be preserved [6,9,13,14].

We acknowledge the support of the GANIL staff and of the AGATA collaboration. This work was partially supported by MCIN/AEI/10.13039/501100011033 and Generalitat Valenciana, Spain, under Grants No. FPA2017-84756-C4, No. PID2020–118265GB-C4, and No. PROMETEO 2019/005, by the EU FEDER funds, by the European Union's Horizon 2020 research and innovation program under Grant Agreement No. n654002, by the U.S. Department of Energy, Office of Science, Office of Nuclear Physics, under Contract No. DE-AC02-06CH11357, by STFC(UK) and by the Croatian Science Foundation under Projects No. 7194 and No. IP-2018-01-1257.

*Corresponding author.
perezvidal@lnl.infn.it

[1] G. Racah, Phys. Rev. **63**, 367 (1943).
[2] G. Racah and I. Talmi, Physica **18**, 1907 (1952).
[3] C. Schwartz and A. de Shalit, Phys. Rev. **94**, 1257 (1954).
[4] A. Arima and H. Kawarada, J. Phys. Soc. Jpn. **19**, 1768 (1964).
[5] A. Arima and M. Ichimura, Prog. Theor. Phys. **36**, 296 (1966).
[6] P. Van Isacker, Int. J. Mod. Phys. E **20**, 191 (2011).
[7] J. J. Valiente-Dobón *et al.*, Phys. Lett. B **816**, 136183 (2021).
[8] A. Escuderos and L. Zamick, Phys. Rev. C **73**, 044302 (2006).
[9] P. Van Isacker and S. Heinze, Phys. Rev. Lett. **100**, 052501 (2008).
[10] A. I. Morales *et al.*, Phys. Rev. C **93**, 034328 (2016).
[11] A. I. Morales *et al.*, Phys. Lett. B **781**, 706 (2018).
[12] T. Marchi, G. deAngelis, J. J. Valiente-Dobon, V. M. Bader, T. Baugher *et al.*, Phys. Rev. Lett. **113** (2014).
[13] A. F. Lisetskiy, B. A. Brown, M. Horoi, and H. Grawe, Phys. Rev. C **70**, 044314 (2004).
[14] A. F. Lisetskiy, B. A. Brown, and M. Horoi, Eur. Phys. J. A **25**, 95 (2005).
[15] L. Zamick and P. Van Isacker, Phys. Rev. C **78**, 044327 (2008).
[16] C. Qi, Phys. Lett. B **773**, 616 (2017).
[17] H. Mach, A. Korgul, M. Gorska, H. Grawe, I. Matea *et al.*, Phys. Rev. C **95**, 014313 (2017).
[18] B. Das *et al.*, Phys. Rev. C **105**, L031304 (2022).
[19] National Nuclear Data Center (ENSDF and XUNDL), https://www.nndc.bnl.gov/.
[20] D. J. Rowe and G. Rosensteel, Phys. Rev. Lett. **87**, 172501 (2001).
[21] C. Qi, Phys. Rev. C **83**, 014307 (2011).
[22] S. Szilner, C. A. Ur, L. Corradi, N. Marginean, G. Pollarolo *et al.*, Phys. Rev. C **76**, 024604 (2007).
[23] M. Siciliano, J. J. Valiente-Dobón, and A. Goasduff, EPJ Web Conf. **223**, 01060 (2019).
[24] R. Broda, C. T. Zhang, P. Kleinheinz, R. Menegazzo, K.-H. Maier, H. Grawe, M. Schramm, R. Schubart, M. Lach, and S. Hofmann, Phys. Rev. C **49**, R575(R) (1994).
[25] M. Siciliano *et al.*, Phys. Lett. B **806**, 135474 (2020).
[26] A. Dewald, O. Möller, and P. Petkov, Prog. Part. Nucl. Phys. **67**, 786 (2012).
[27] S. Akkoyun *et al.*, Nucl. Instrum. Methods Phys. Res., Sect. A **668**, 26 (2012), and references therein.
[28] E. Clément *et al.*, Nucl. Instrum. Methods Phys. Res., Sect. A **855**, 1 (2017).
[29] S. Pullanhiotan, M. Rejmund, A. Navin, W. Mittig, and S. Bhattacharyya, Nucl. Instrum. Methods Phys. Res., Sect. A **593**, 343 (2008).
[30] M. Rejmund *et al.*, Nucl. Instrum. Methods Phys. Res., Sect. A **646**, 184 (2011).
[31] P.-A. Söderström *et al.*, Nucl. Instrum. Methods Phys. Res., Sect. A **638**, 96 (2011).
[32] A. López-Martens, K. Hauschild, A. Korichi, J. Roccaz, and J.-P. Thibaud, Nucl. Instrum. Methods Phys. Res., Sect. A **533**, 454 (2004).
[33] R. M. Pérez-Vidal, Ph.D thesis, Universidad de Valencia, 2019, https://roderic.uv.es/handle/10550/72450.
[34] S. Pullanhiotan, A. Chatterjee, B. Jacquot, A. Navin, and M. Rejmund, Nucl. Instrum. Methods Phys. Res., Sect. B **266**, 4148 (2008).
[35] M. Vandebrouck, A. Lemasson, M. Rejmund, G. Fremont, J. Pancin, A. Navin, C. Michelagnoli, J. Goupil, C. Spitaels, and B. Jacquot, Nucl. Instrum. Methods Phys. Res., Sect. A **812**, 112 (2016).
[36] M. Rejmund, S. Bhattacharyya, A. Navin, W. Mittig, L. Gaudefroy, M. Gelin, G. Mukherjee, F. Rejmund, P. Roussel-Chomaz, and C. Theisen, Phys. Rev. C **76**, 021304(R) (2007).
[37] D. Mengoni, J. J. Valiente-Dobón, E. Farnea, A. Gadea, A. Dewald, and A. Latina (CLARA-PRISMA Collaboration), Eur. Phys. J. A **42**, 387 (2009).
[38] C. Stahl, J. Leske, M. Lettmann, and N. Pietralla, Comput. Phys. Commun. **214**, 174 (2017).
[39] A. Blazhev, M. Gorska, H. Grawe, J. Nyberg, M. Palacz *et al.*, Phys. Rev. C **69**, 064304 (2004).
[40] J. Park *et al.*, Phys. Rev. C **96**, 044311 (2017).
[41] J. Park *et al.*, Phys. Rev. C **103**, 049901(E) (2021).
[42] E. Caurier, G. Martínez-Pinedo, F. Nowacki, A. Poves, and A. P. Zuker, Rev. Mod. Phys. **77**, 427 (2005).

[43] L. Coraggio, L. De Angelis, T. Fukui, A. Gargano, N. Itaco, and F. Nowacki, Phys. Rev. C **100**, 014316 (2019), and references therein.
[44] K. Suzuki and R. Okamoto, Prog. Theor. Phys. **93**, 905 (1995).
[45] L. Coraggio and N. Itaco, Front. Phys. **8**, 345 (2020).
[46] P. Van Isacker, J. Phys. **322**, 012003 (2011).
[47] S. Cohen, R. D. Lawson, M. H. Macfarlane, and M. Soga, Phys. Lett. **10**, 195 (1964).